Catalysis Science & Technology

ROYAL SOCIETY OF CHEMISTRY

PAPER

View Article Online
View Journal | View Issue

Cite this: *Catal. Sci. Technol.*, 2022, **12**, 3044

Effect of cobalt doping on photocatalytic water splitting activity of NiTi-layered double hydroxide†

Sara Samuei, [a] Sina Sadigh Akbari, [a] Emine Ülker[b] and Ferdi Karadas *[ac]

Received 22nd January 2022,
Accepted 17th March 2022

DOI: 10.1039/d2cy00148a

rsc.li/catalysis

Metal doping has been used as an effective strategy to tune the energy levels of semiconductors. Herein, we dope NiTi layered double hydroxide (NiTi-LDH) with cobalt to prepare a ternary LDH, CoNiTi-LDH, to enhance its photocatalytic performance towards both water oxidation and hydrogen evolution. A CoNiTi-LDH with smaller plate sizes and a higher degree of order is obtained, which allows the band gap to shrink from 2.7 eV to 2.4 eV. CoNiTi-LDH exhibits a photocatalytic water oxidation activity of 366 μmol g^{-1} h^{-1}, which is more than two times higher than NiTi-LDH (166 μmol g^{-1} h^{-1}). We observed that appropriate energy levels of CoNiTi-LDH allow it to be an efficient photocatalyst also for hydrogen evolution. We performed detailed characterization studies to elucidate the effect of Co-doping on photocatalytic activity.

Introduction

Solar energy-driven water splitting promises a sustainable pathway for clean and renewable energy.[1,2] One of the critical steps in advancing sustainable water splitting cells is the development of an efficient semiconductor.[3] Although the fundamentals of this field have been mainly established with TiO_2, its large bandgap (>3 eV) limits its efficiency in harvesting visible light.[4,5] Various attempts have been employed to develop efficient semiconductors, including modified $NaTaO_3$, $SrTiO_3$, Ga_2O_3, C_3N_4, GaN, and ZnO.[6–8] Recently, protective layers such as Al_2O_3 and TiO_2 have been utilized to boost the stability of photocatalysts over long reaction periods.[9,10] An ideal semiconductor with appropriate energy levels to absorb visible light and inject holes and electrons to suitable components should be designed to advance sustainable water splitting cells. The band gap is a critical parameter that defines the solar light-harvesting capacity of a semiconductor. The visible and near-infrared wavelengths make up the majority of solar light energy, with the UV range accounting for only around 5%. Unfortunately, most visible-light absorbing semiconductors are unstable, leading to deactivation over time. Chen *et al.*[11] reported that coupling noble metals with bare TiO_2 could dramatically increase visible light absorption.[12] Furthermore, defect engineering[13] and the coupling of two different semiconductors[14,15] have been examined. In addition to efficient solar light harvesting, a suitable water splitting photocatalyst should have a suitable conduction band (CB) to facilitate electron for H_2 evolution (0.000 V *vs.* NHE at pH 0) and a suitable valence band (VB) to utilize photogenerated holes for water oxidation (1.23 V *vs.* NHE at pH 0).[16,17]

Layered double hydroxides (LDHs) constitute a potential alternative for TiO_2-based photocatalysts. They show high surface area, low preparation cost, a facile synthetic pathway that allows easy tuning of composition, and electronic properties that provide convenient migration and separation of the photogenerated charge carriers.[18] Moreover, the surface hydroxyl groups of LDHs could react with valence band holes to produce hydroxyl radicals ($OH^{\bullet}$) that participate in the oxidation process as a key intermediate species.[18,19]

LDHs are represented with a general formula of $[M^{2+}_{1-x}M^{3+}_{x}(OH)_2]^{x+}(A^{n-})_{x/n}{\cdot}mH_2O$, where M^{2+} and M^{3+} are the metal cations, and A^{n-} is the interlayer anion.[18,20] The structure of LDHs is mainly based on brucite-like ($Mg(OH)_2$) layers, including edge-shared octahedral parts surrounded by hydroxyl groups.[21,22] Many transition metal ions in their +2 and +3 oxidation states could easily be incorporated into an LDH structure. Various pure and modified LDHs have been studied to elucidate the effect of metal content and ratio on the energy levels and charge separation efficiency. Recently, it has also been found that Ti-based LDHs could also be prepared, in which Ti is in a +3/+4 mixed oxidation state.

Ti-based LDHs have received attention due to their appropriate energy levels with respect to water oxidation and reduction processes. Wei *et al.* demonstrated that Ti-based LDHs could be visibly active for photocatalytic oxygen

[a] *Department of Chemistry, Faculty of Science, Bilkent University, Ankara 06800, Turkey. E-mail: karadas@fen.bilkent.edu.tr*
[b] *Department of Chemistry, Faculty of Arts & Science, Recep Tayyip Erdogan University, Rize, Turkey*
[c] *UNAM – National Nanotechnology Research Center, Institute of Materials Science and Nanotechnology, Bilkent University, Ankara 06800, Turkey*

† Electronic supplementary information (ESI) available. See DOI: https://doi.org/10.1039/d2cy00148a

production by increasing electron–hole separation.[23] A ZnAlTi ternary layered double hydroxide was shown to exhibit excellent performance for the degradation of pollutants and decomposition of water under visible-light irradiation.[24] By investigating Ti-based LDHs as heterometallic photocatalysts, Frei *et al.* concluded that forming Ti^{3+} active sites can act as trapping sites for effective electron–hole separation.[25] Additionally, these LDHs can react in the visible region by narrowing the semiconductor bandgap.[25,26] In another study by Wei *et al.*, NiTi LDH nanosheets were utilized as efficient photocatalysts for the water oxygen process.[26] Photocatalytic hydrogen evolution with a Ti-based LDH, however, has not been achieved to date.

Efforts to enhance the photocatalytic activity of Ti-based LDHs in the visible region are centered mainly on changing synthetic methods such as hydrothermal synthesis and microemulsion method. Metal ion doping is another common approach to prepare efficient visible-light-driven Ti-LDHs. Studies reveal that oxo-metal bonds between two or three different metal ions in LDHs can act as TiO_2 doping materials.[27,28] Garcia *et al.* studied a series of visibly active LDH catalysts containing Zn/M (M = Cr, Ti, Ce). They demonstrated that Cr could be used as a dopant for the water-splitting process.[29] Dopants can improve the performance of photocatalysts by improving the dispersion degree of the MO_6 octahedral particles and/or the number of defects, which are crucial for the efficiency of a semiconductor. Dispersion degree enhancement facilitates electron transfer by preventing the recombination of electrons and holes.[30–33] Metal doping in LDHs, thus, provides a facile and straightforward pathway to change the coordination environment around the metal by altering the M–O bond for hydroxides/oxides.[34,35] This alteration in the structure creates oxygen vacancies that improve catalytic activity.[36] Oxygen vacancies around the metal sites create active non-coordinated sites, increasing the conductivity and accelerating the electron transfer in the OER.[37,38] Liu and coworkers used a co-doping strategy to control the oxygen vacancy formation of NiFe-LDH for superior OER and HER activity. Co-doping can weaken the bond between the metal and oxygen atoms and could lead to an increase in the number of oxygen vacancies due to charge balance.[39] An oxygen vacancy typically enhances the catalytic activity by boosting the number of uncoordinated metal centers, which are presumed as the real active sites for a catalytic process.[40] Moreover, such vacancies could tune the electronic states that affect electron transfer and electron–hole recombination pathways.[37] High-performance photocatalysts also exhibit low-dimensionalities with porous nature, as they have fewer mass transfer constraints.[41]

Based on the results obtained from this study, the band center of O 2p shifts to the Fermi level after co-doping, indicating the formation of oxygen vacancies. By increasing the oxygen vacancies, the size of particle samples decreases, which leads to the increase of accessible photocatalytic active sites around oxygen vacancies. The catalytic activity is, thus, enhanced due to efficient charge transfer in the OER and HER.

In this research work, we prepared cobalt-doped NiTi LDHs by a coprecipitation method. Previous studies in this field reveal that cobalt doping yields oxygen vacancies, which minimizes the recombination of the charge carrier center lowering the bandgap to harvest the visible light more efficiently.[42,43] We employed a Ti-based LDH for the first time for both photocatalytic oxygen evolution and hydrogen evolution processes to the best of our knowledge. We performed comprehensive studies to evaluate the effect of cobalt-doping on the catalytic performance and the band gap of the LDH.

Experimental

Reagents

All the used chemical materials, including $Ni(NO_3)_2{\cdot}6H_2O$, $Co(NO_3)_2{\cdot}9H_2O$, and $TiCl_4$, were of analytical grade and purchased from Merck or Sigma Aldrich Company, and the synthesis steps were performed using deionized water. The pH values were adjusted by adding different amounts of the 0.1 M solution of NaOH and 0.1 M solution of HCl.

Apparatus

Powder X-ray diffraction (PXRD) spectra of the samples were recorded using a Panalytical X'pert Multi-Purpose diffractometer at the range of 2θ = 10–70 using Bragg–Brentano geometry (Cu Ka radiation; l = 0.15418 nm). A Bruker ALPHA Platinum-ATR spectrometer in the wavenumber range 4000–400 cm^{-1} was used to obtain the Fourier transform infrared (FTIR) spectra.

The pH values were adjusted with a Mettler-Toledo AG pH meter model 8603. The morphologies of the prepared nanocomposites were investigated with a scanning electron microscope (SEM, FEI e Quanta 200 FEG) operated at 10 kV. A transmission electron microscope (TEM, Tecnai G2-F30, FEI) was used at 200 kV combined with an energy dispersive X-ray spectrometer (EDS) to obtain the chemical composition of synthesized materials. The samples were prepared by partially dispersing the materials in water by ultrasonication and depositing a drop of the dispersed material on a copper grid. X-ray Photoelectron (XPS) measurements were performed using an X-ray photoelectron spectrometer system (Thermoscientic KAlpha, $h\nu$ = 1486.6 eV). Electrochemical studies were performed at room temperature using a Gamry Interface 1000 potentiostat/galvanostat instrument with a three-electrode system. A glassy carbon electrode, a silver/silver chloride electrode [Ag/AgCl/KCl (Sat)], and a Pt wire electrode are the working, reference, and counter electrodes, respectively. Surface area analysis was performed using a Quantochrome Autosorb IQ_2 MP gas sorption system. UV-visible DRS results were obtained with the NWs using a UV-vis-NIR spectrophotometer (Cary 5000, Varian). The electrolyte solution was saturated with N_2 gas for 30 min to remove the dissolved O_2 gas before each measurement. A

solar light simulator (ABET, Model 10 500. US Pat. No. 8116017, DC Xe Arc lamp, AM 1.5 global filter) was calibrated to 1 sun (100 mW cm^{-2}) using a thermopile optical detector (Newport, Model 818P-010-12).

Synthesis of NiTi-LDH

The NiTi-LDH sample was prepared by the coprecipitation method.[44] In brief, a 0.5 mL $TiCl_4$: HCl solution {1 : 1 (v/v)}, and $Ni(NO_3)_2{\cdot}6H_2O$ (0.008 mol) were dissolved in deionized water under vigorous stirring. The pH of the reaction mixture was maintained at 9 using 0.1 M NaOH solution under a N_2 atmosphere. The solution was kept at 70 °C for 24 h. The resulting slurry was then centrifuged, washed three times with distilled water, and dried at 60 °C.

Synthesis of CoNiTi-LDH

The synthesis of the CoNiTi-LDH sample was according to the procedure mentioned above with a modification in the ratio of materials $Ni(NO_3)_2{\cdot}6H_2O$, $Co(NO_3)_2{\cdot}6H_2O$ and $TiCl_4$ of 1 : 1 : 2. The pH of the solution was adjusted to 10 by using 0.1 M NaOH solution under a N_2 atmosphere. The solution temperature was maintained at 70 °C and kept for 24 h. The resulting precipitate was then centrifuged, rinsed three times with distilled water, and dried at 60 °C.

Photocatalytic experiments

Photocatalytic experiments were performed in a 10 mL Pyrex reactor at room temperature. A 10 mg of catalyst was dispersed in 10 mL water containing 10 mM $AgNO_3$ as a sacrificial agent. The reactor was sealed perfectly airtight with septa. Before the photocatalytic experiment, the reaction solution was purged thoroughly with N_2 to remove O_2. The solar simulator (ABET, Model 10 500. US Pat. No. 8116017, DC Xe Arc lamp, AM 1.5 global filter) was used as a light source. Oxygen evolution investigations were followed by injecting 100 μL of the reactor headspace gas into a gas chromatograph (Agilent 7820 A GC) equipped with a Molesieve column and a TCD detector with Ar as carrier gas. Sampling was performed at specified intervals, and the experiments were repeated for reproducibility. Characterization experiments involving XRD, XPS, and FT-IR analysis were also performed for the samples after photocatalytic experiments.

Results and discussion

Both samples were prepared by the coprecipitation method. Nitrate salts and the $TiCl_4$:HCl solution were used as precursors after pH and temperature adjustment and kept at least 24 hours. It is worth noting that the type of cation, their molar ratios, and the nature of interlayer anions yield various types of LDHs with unique physical and chemical properties. Varying the type of metal, thus, changes the band gap and band edge positions.[45,46]

The formation of the LDH structure is confirmed by XRD studies (Fig. 1a). Unit cell reflections are indexed to a rhombohedral *R*3*m* symmetry for both samples, typical for the LDH structure.[22] The characteristic peaks of the LDH structure (LDH: JCPDS File No. 38-487)[39] for the (003), (006), (012), and (015) crystallographic planes are observed for both samples. Lattice parameters, $a = 2d_{110}$ and $c = 3d_{003}$, are determined as 3.08 and 21.6 Å for NiTi-LDH and 3.04 and 23 Å for CoNiTi-LDH, using the (003), (006), and (110) planes.[39,47] The increase in the intensity and the sharpening of the (003) and (006) diffraction peaks of CoNiTi-LDH suggest a higher degree of plane stacking than that of NiTi-LDH. No extra characteristic peaks were detected from XRD patterns, indicating no impurities in the products.[21,48] On the other hand, a decrease in the intensity of the (015), (018), and (113) planes reveals a decrease in the layer size for CoNiTi-LDH, which is also observed with TEM studies. An average plate size of 50 nm is obtained for NiTi-LDH, while it is around 10 nm for the cobalt-doped one. TEM images also reveal an interplanar distance of 0.51 nm, which matches the d_{110} of CoNiTi-LDH (0.51 nm, 2θ = 61.25°) and NiTi-LDH

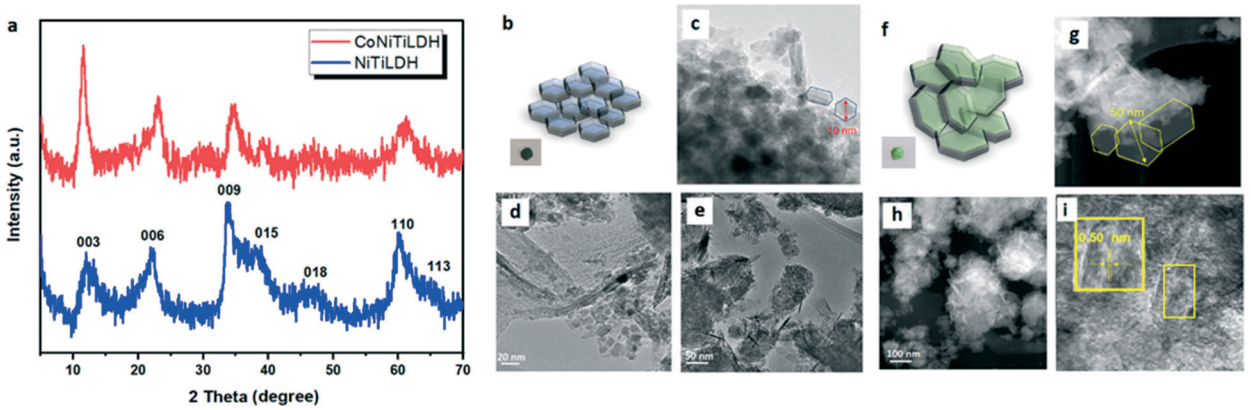

Fig. 1 (a) XRD patterns of CoNiTi-LDH and NiTi-LDH samples. (b) Schematic representation and (c–e) TEM micrographs of the CoNiTi-LDH sample. (f) Schematic representation and (g–i) TEM micrographs of the NiTi-LDH sample with an interlayer distance of 0.50 nm, compatible with the (110) plane calculated by Bragg's law.

(0.50 nm, 2θ = 60.07°).[48] TEM analysis was performed to investigate the morphology of the samples (Fig. 1b–i). TEM images reveal the presence of ultra-fine hexagonal nanoparticles stacked on each other, mostly in a vertical alignment, accompanied by an inevitable aggregation for both samples.

Moreover, CoTiNi-LDH exhibits smaller particle sizes and a lower degree of aggregation than NiTi-LDH. The interplanary distance calculated by the magnification of the TEM image of NiTi-LDH corresponds to the (110) plane, which was not detectable for CoNiTi-LDH (Fig. 1i). Similarly, a comparison of powder XRD patterns reveals that the diffraction peak for the (110) planes exhibits a lower intensity for CoNiTi-LDH, which could be attributed to the smaller particle size of CoNiTi-LDH than NiTi-LDH. Fig. 1b and f illustrate the schematic diagram of the morphologies of both samples for clarity based on TEM and XRD analysis. Delaminated LDH structures were also observed for both samples when treated with butanol (Fig. S1†).

The FT-IR spectra of CoNiTi-LDH and NiTi-LDH exhibit similar profiles (Fig. S2†). The broad and intense absorption peaks of O–H are observed at around 3400 cm^{-1}. A relative broadening is observed due to the hydrogen bond between the surface hydroxyl groups of the LDH structure and the interlayer water molecules. The band at 1640 cm^{-1} for both samples corresponds to the H–O–H bending mode. The M–O stretching vibrations are below 1000 cm^{-1}.[49] The peaks centered at 575 cm^{-1} and 440 cm^{-1} belong to M–O–H and O–M–O, respectively.[20,50] The band at 1384 cm^{-1} corresponds to the stretching modes of nitrate anions located in the interlayer space.[51] The additional absorption bands in the 1375–1450 cm^{-1} region imply the presence of carbonate groups available in the interlayers, which could be absorbed during the aging process.

The morphology investigation of the samples performed by SEM imaging analysis reveals partial aggregation, which is relatively higher in NiTi-LDH (Fig. S3†). The particles are regular and detectable individually for both samples. The decrease in the agglomeration and the plate size with cobalt-doping observed by both TEM and SEM analysis suggests an increase in the surface area, which is desired for enhancing photocatalytic activity.[52] The surface area analysis with the BET technique confirms that Co-doped LDH has a higher surface area (340 $m^2\ g^{-1}$) than NiTi-LDH (291 $m^2\ g^{-1}$). CoNiTi-LDH, thus, provides more active adsorption sites and photocatalytic active centers.[53]

The EDX analysis associated with the elemental composition yields an atomic ratio of Co : Ni : Ti = 0.2 : 0.2 : 1 and Ni : Ti = 0.8 : 1 for CoNiTi-LDH and NiTiLDH, respectively (Fig. S4†). Thermogravimetric analysis (TGA) and differential thermal analysis (DTA) reveal a two-step decomposition for both CoNiTi-LDH and NiTi-LDH (Fig. S5†). The first step that spans a temperature range of 50–180 °C involves the release of water molecules from the surface and the LDH interlayer, while the one in the 180–350 °C range corresponds to the dehydroxylation of brucite-like octahedral layers to form oxides.[54] The compounds exhibit two separate peaks in the DTA profile. The first peak below 100 °C is attributed to the release of physically adsorbed water molecules. An increase in its intensity for CoNiTi-LDH suggests that cobalt-doping increases the surface area, thus increasing the number of interlayer water molecules. According to the literature, LDHs have the ability to absorb water, which allows them to reach the intergallery space as well as the exterior non-gallery surface, maximizing the surface area of the material for photocatalysis and oxygen generation.[55] Thus, in the case of CoNiTi-LDH, the higher percentage of absorbed water suggests the improved water-splitting efficiency of this sample compared to NiTi-LDH.

The chemical compositions of the NiTi-LDH and CoNiTi-LDH samples were also investigated by X-ray photoelectron spectroscopy (XPS) (Fig. 2). The Ni 2p spectrum of the NiTi-LDH sample displays two typical Ni^{2+} $2p_{3/2}$ and Ni^{2+} $2p_{1/2}$ peaks located at 855.2 eV and 872.8 eV, respectively.[56]

The shake-up satellite peaks are also observed at higher binding energies. The Ti spectrum of the NiTi-LDH sample exhibits two peaks at binding energies of 457.9 eV and 463.7 eV corresponding to Ti $2p_{3/2}$ and $2p_{1/2}$, respectively, indicating the presence of Ti^{4+} in the $Ti(OH)_6$ structure.[57] Co-doping of the LDH layers does not significantly change the Ni 2p and Ti 2p profiles (Fig. 2a and b). In the high-resolution O 1s spectrum of the NiTi-LDH sample, there are three peaks at binding energies of 529.5 eV, 530.6 eV, and 531.8 eV, which can be assigned to the lattice oxygen, the hydroxyl group in LDH layers, and carbonate groups, respectively.[58,59] For the CoNiTi-LDH sample, these peaks were observed at 529.5 eV, 530.8 eV, and 532.1 eV (Fig. 2c). The Co $2p_{3/2}$ and Co $2p_{1/2}$ signals can be deconvoluted into two primary peaks with shake-up satellite peaks at higher binding energies. Previous studies show that the Co $2p_{3/2}$–Co $2p_{1/2}$ spin-orbit splitting is 15 eV for Co(III) complexes and 16 eV for Co(II) complexes.[60,61] The presence of satellite peaks and a binding energy difference of 15.5 eV confirms the co-existence of Co(III) and Co(II) oxidation states in the CoNiTi-LDH structure (Fig. 2d). XPS profiles were also studied to investigate the stability of the NiTi-LDH and CoNiTi-LDH samples. Ni 2p and Ti 2p regions remain unchanged during the photocatalytic experiment for the NiTi-LDH sample (Fig. S6a and b†). Meanwhile, the post-catalytic O 1s spectrum indicates that the content of carbonate groups on the surface of NiTi-LDH increases (Fig. S6c†). The Ni 2p and O 1s spectra of the pristine and post-catalytic samples of CoNiTi-LDH display similar profiles, while the binding energies of Ti 2p exhibit slightly positive shifts after the photocatalytic process (Fig. 3a–c). The lower intensity of Co $2p_{3/2}$ and Co $2p_{1/2}$ satellites in the post-catalytic sample suggests that the cobalt cations with the +2 oxidation state are partially oxidized to the +3 oxidation state over the photocatalytic experiment (Fig. 3d).[61,62]

A suspension containing the powder catalyst and $AgNO_3$ as a sacrificial agent was irradiated with visible light to evaluate the photocatalytic water oxidation activity.[63] Co-

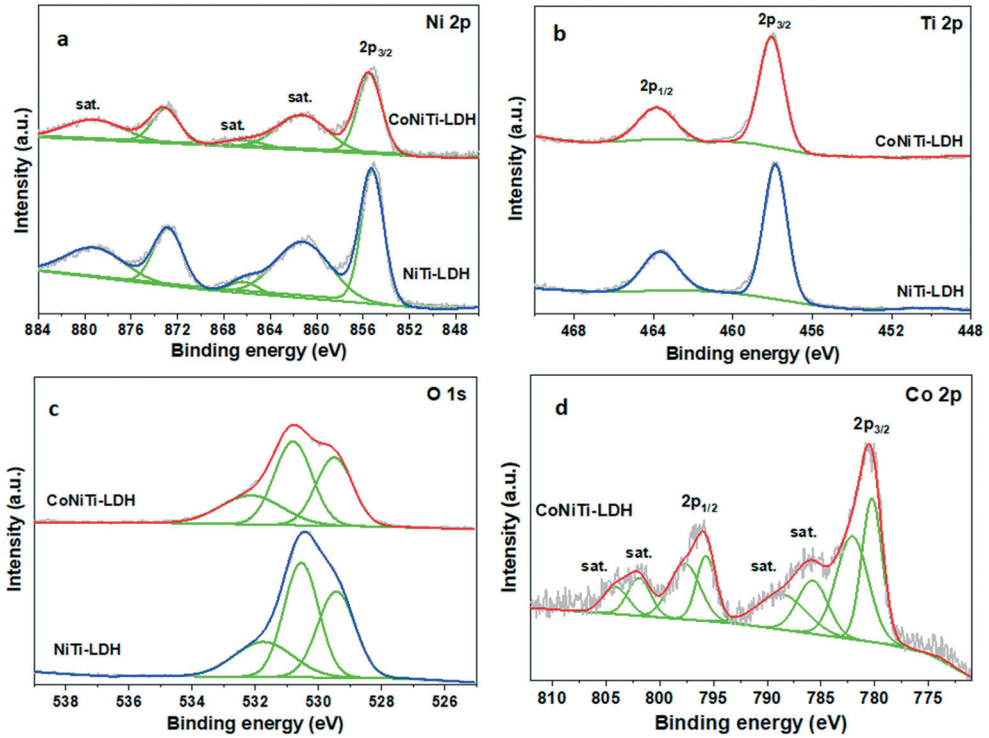

Fig. 2 XPS spectra of the CoNiTi-LDH and NiTi-LDH samples: (a) Ni 2p; (b) Ti 2p; (c) O 1s, and (d) Co 2p.

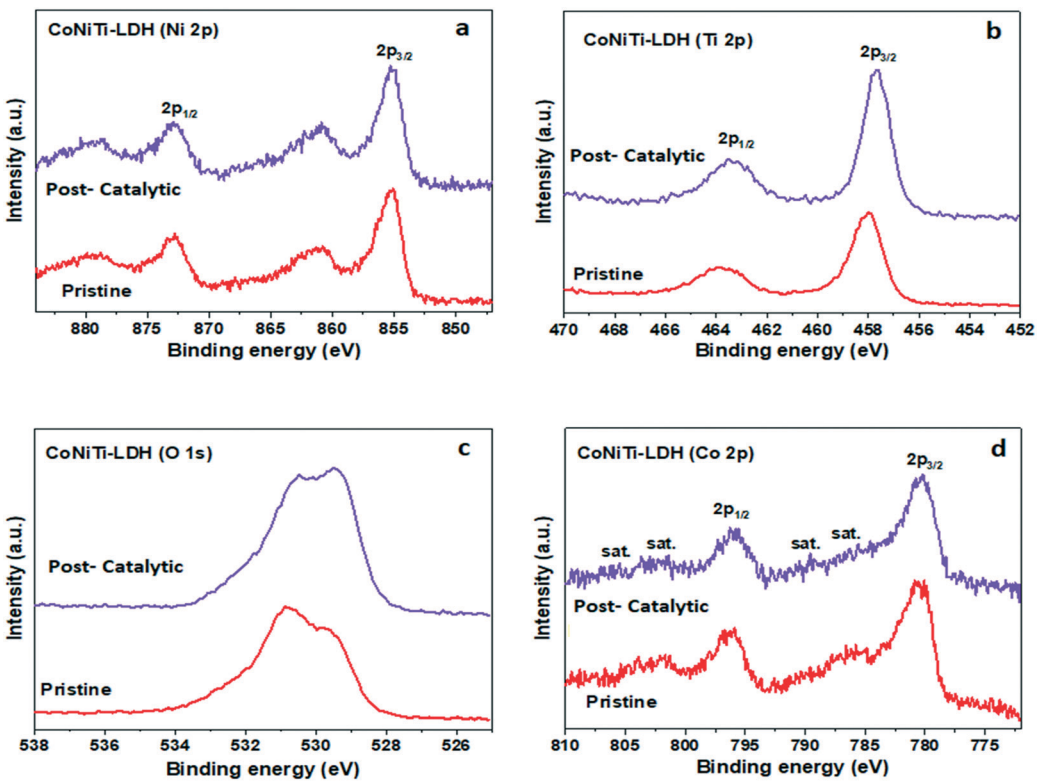

Fig. 3 XPS spectra of CoNiTi-LDH for pristine and post-catalytic samples: (a) Ni 2p, (b) Ti 2p, (c) O 1s, and (d) Co 2p.

doped NiTiLDH exhibits an activity of 366 μmol g^{-1} h^{-1}, which is more than two times higher than NiTi-LDH (161 μmol g^{-1} h^{-1}) (Fig. 4a). Metal doping has been reported to alter the surface structure of LDHs, the energy levels, the electron–hole recombination rate, and the defects in the crystalline structure. As a result, the type and the amount of

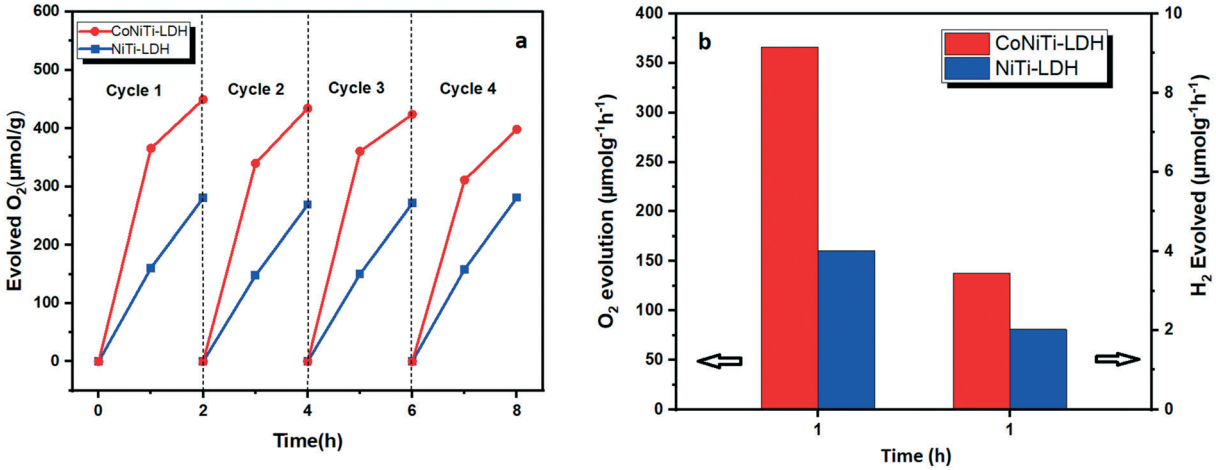

Fig. 4 (a) Photocatalytic O_2 generation rate through four consecutive cycles for CoNiTi-LDH and NiTi-LDH samples in H_2O containing 10 mg catalyst and 10 mM $AgNO_3$ as the sacrificial agent under visible light irradiation. After each cycle, 10 mM $AgNO_3$ was added to the reaction solution. (b) Comparison of the photocatalytic activity for O_2 and H_2 evolution of CoNiTi-LDH and NiTi-LDH samples. 10 mM $AgNO_3$ and methanol were used as sacrificial agents for photocatalytic O_2 and H_2 evolution experiments, respectively.

dopant affect the photocatalytic activity.[64,65] For example, the incorporation of lanthanum (La) as an additive or dopant into a CoAl-LDH changes the crystal structure due to the formation of a vacancy-rich ternary CoAlLa-LDH. This change enhances the photocatalytic activity by improving the active sites to promote photogenerated charge separation.[66]

Furthermore, a four-cycle photocatalytic experiment reveals that the activity of NiTi-LDH remains almost constant while a minor decrease (3.4% change) is observed for Co-doped NiTi-LDH at each cycle. This slight decrease could be attributed to the partial inhibition of the catalyst surface due to the formation of Ag nanoparticles from the sacrificial agent, as confirmed by XRD studies performed on the post-catalytic samples (Fig. S7†).

The XRD pattern of post-catalytic CoNiTi-LDH reveals a set of new diffraction patterns with high intensity, which is attributed to the formation of Ag nanoparticles due to the reduction of Ag^+ ions that serve as an electron scavenger (Fig. S7†).[67,68] The peak that belongs to Ag nanoparticles has a weaker intensity for NiTi-LDH since fewer Ag^+ ions are consumed due to the lower photocatalytic activity of NiTi-LDH compared to CoNiTi-LDH. Infrared studies are also performed on the post-catalytic samples (Fig. S8†). The appearance of the N–O band at 1530 cm^{-1} is attributed to the nitrate of $AgNO_3$ and the interlayer anion of LDHs.

The bands around 3444 cm^{-1} are assigned to the O–H stretching vibrations. The shoulders at 2856 cm^{-1} and 2910 cm^{-1} could be indexed to the H-bonding arising between the H_2O and CO_3^{2-} anions.[69] The slight differences in the infrared spectra of pristine and post-catalytic samples could be explained by the alteration of the surface due to the formation of Ag nanoparticles on the surface. The formation of Ag nanoparticles, thus, does not lead to a major structural change in LDHs. All functional groups, including hydroxyl groups, are still retained.[70] The structural integrity of LDHs during the photocatalytic process could also be confirmed by the constant activity profile during a four-cycle photocatalytic experiment.

The photocatalytic activities of the samples were compared to other LDH-based photocatalysts in the literature (Table S1†).[44,71–78] Table S1† clearly indicates that the performance is mainly governed by the synthetic method and, thus, the structure. For example, Kong *et al.* show that as the number of surface defects in the structure is enhanced, the photogenerated electron–hole separation efficiency increases, which leads to an enhancement in the photocatalytic activity.[79] We also employed a similar synthetic method to prepare LDHs. Cobalt ions are incorporated into the LDH structure in this study to improve charge separation. Moreover, as confirmed by BET and TEM results, Co-doping increases the surface area and prevents aggregation, which helps to improve the photocatalytic activity.

The photocatalytic hydrogen evolution activities of LDHs were also investigated in the presence of methanol as a sacrificial agent (Fig. 4b). Although the activities are not as high as oxygen evolution, both LDHs are active for hydrogen evolution for the first time to our knowledge.

A combination of UV-vis spectroscopy and electrochemical experiments is performed to establish the band energy alignment for LDHs. UV-vis diffuse reflectance experiments indicate that NiTi-LDH exhibits an absorbance in the UV region with an absorption edge of around 500 nm and a broad absorption band in the 600–800 nm range (Fig. 5a). On the other hand, the absorption profile of CoNiTi-LDH in the UV region is extended to higher wavelengths. Furthermore, it exhibits a more intense absorbance in the visible region, desired for photocatalytic applications.[80,81] Three distinct peaks in the visible region are also introduced to the absorption profile with the addition of cobalt ions to the LDH structure. These absorption bands correspond to d–d transitions of Co^{2+} and Co^{3+} ions. The first absorption band at 550 nm is assigned to the $^5T_{2g} \rightarrow E_g$ transition of Co^{3+} ions

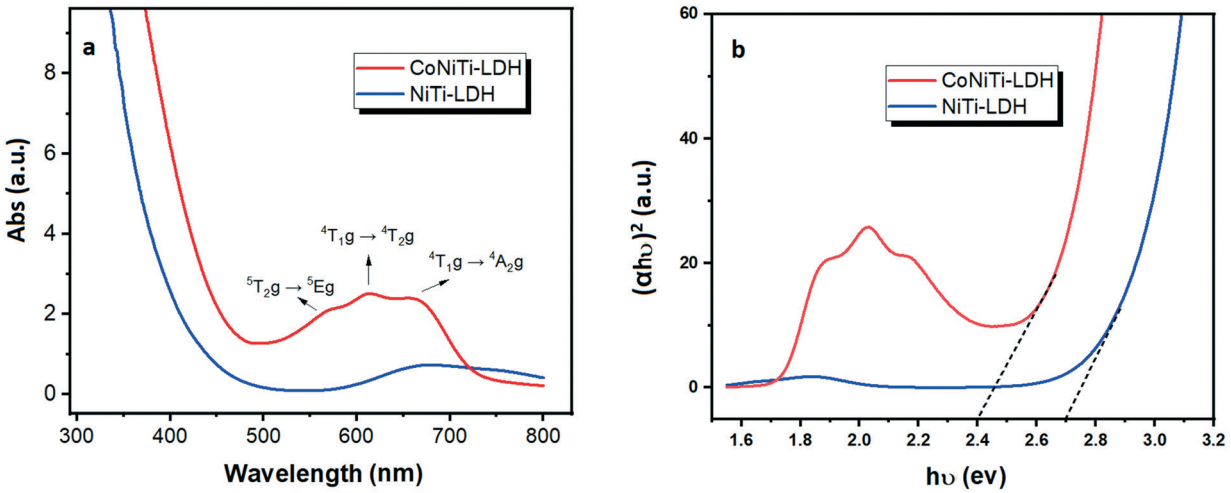

Fig. 5 (a) Diffuse reflectance UV-vis spectra (plotted as the Kubelka–Munk function of the reflectance, *R*) of the CoNiTi-LDH and NiTi-LDH samples. (b) Tauc's plots of the CoNiTi-LDH and NiTi-LDH samples for band gap estimation.

while the other bands at 600 and 670 nm correspond to $^4T_{1g} \rightarrow {}^4T_{2g}$ and $^4T_{1g} \rightarrow {}^4A_{2g}$ d–d transitions in Co^{2+} ions. Although there are three possible transitions for Co^{2+} ions, due to the high energy transition of $^4T_{1g} \rightarrow {}^4T_{1g}(P)$, only two distinctive peaks are observed ($^4T_{1g} \rightarrow {}^4T_{2g}$ and $^4T_{1g} \rightarrow {}^4A_{2g}$).[82,83] The absorbance profile, thus, confirms the presence of a combination of Co^{2+} and Co^{3+} ions in CoNiTi-LDH, as also observed by XPS analysis.

The band gaps of LDHs were found based on the fitting of absorption data with Tauc's equation $[(\alpha h\nu)^{1/n} = A(h\nu - E_g)]$ where α, h, ν, A, and E_g are the absorption coefficients, Planck's constant, light frequency, proportionality constant, and band gap energy, respectively. A semiconductor could be fitted as either an indirect band gap one ($n = \frac{1}{2}$ for direct allowed transition) or a direct band gap one ($n = 2$ for indirect allowed transition).[84] For both CoNiTi-LDH and NiTi-LDH, the curves of $(\alpha h\nu)^2$ *vs.* $h\nu$ plot are linear (Fig. 5b), which suggests that they can be treated as direct band gap semiconductors. The calculated band gaps reveal that CoNiTi-LDH exhibits a narrower band gap (2.4 eV) than NiTi-LDH (2.7 eV).

Cyclic voltammetry experiments were performed to estimate the energy levels of LDHs (Fig. S9†).[84] As presented in Fig. 6, HOMO levels of CoNiTi-LDH and NiTi-LDH are obtained as around 1.1 V and 1.4 V *vs.* NHE, respectively.

The proposed structural model of energy states for Co-doped NiTi-LDH and NiTi-LDH is illustrated in Fig. 6. Electrons and holes are created in the CB and VB when the semiconductor is photoexcited. As shown in Fig. 6, the VBs of both CoNiTi-LDH and NiTi-LDH are positioned below the

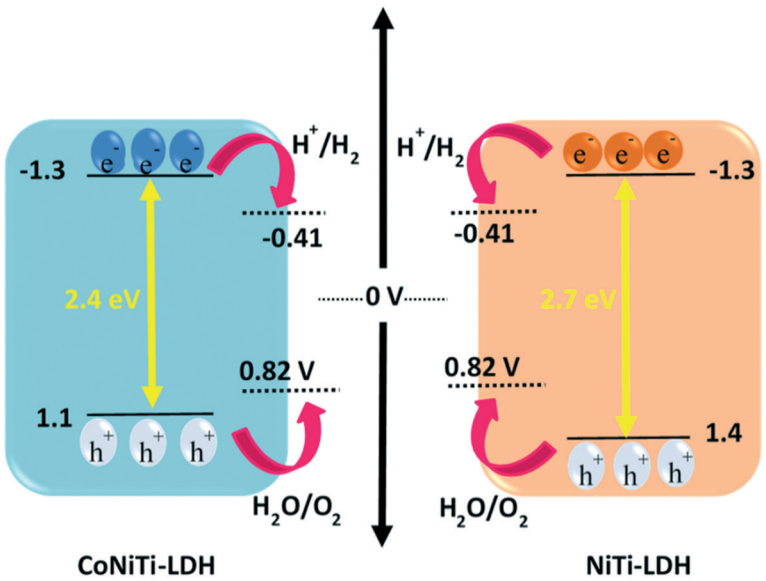

Fig. 6 Schematic representation of the CoNiTi-LDH and NiTi-LDH (V *vs.* NHE at pH = 7) estimated band structure involving the electron-transfer mechanism.

water oxidation potential as desired. The CoNiTi-LDH sample possesses a better band energy alignment compared to NiTi-LDH since the VB of CoNiTi-LDH is much closer to the water oxidation level. The enhancement in the water oxidation activity with Co-doping could, thus, be attributed to the decrease in the bandgap (better absorption in the visible region) and the decrease in the energy difference between the VB and the water oxidation potential (better charge transfer). Band alignment diagrams also reveal that the CBs of LDHs are higher in energy than the H_2 evolution potential. The relatively low photocatalytic activity towards water reduction could be attributed to the relatively large energy difference between the CB and the H_2 evolution potential. Previous studies also support our experimental findings; doping could alter the crystal lattice modification to reduce the bandgap and improve the visible light absorption capacity. Doping with suitable cations could also create additional adsorption sites for reactants and produce lattice defects that increase the charge separation efficiency.[85,86] Furthermore, increased surface area improves accessible active catalytic sites.[87] Overall, metal doping has been a viable strategy to optimize the structural, optical, and textural features of LDHs and for the preparation of an LDH with a desired thickness, size, surface area, and active site.

Conclusions

In conclusion, we doped NiTi-LDH with cobalt ions to prepare CoNiTi-LDH. CoNiTi-LDH consists of smaller nanoplates (10 nm) with less aggregation than NiTi-LDH (50 nm). CoNiTi-LDH also exhibits a higher surface area (340 $m^2\ g^{-1}$) than NiTi-LDH (291 $m^2\ g^{-1}$). These changes in the structure and morphology of LDH lead to a significant enhancement in the photocatalytic water oxidation activity 366 μmol $g^{-1}\ h^{-1}$ for CoNiTi-LDH and only 161 μmol $g^{-1}\ h^{-1}$ for NiTi-LDH. Both LDHs are also found to be active for the hydrogen evolution reaction with an activity of around 3.4 μmol $g^{-1}\ h^{-1}$. A combination of experimental studies was performed to elucidate the enhancement of activity with Co-doping. Our studies reveal that the VB level of LDH is upshifted to around 1.1 eV and positioned closer to the oxidation level of water with Co-doping.

Moreover, the band gap is widened (2.4 eV for CoNiTi-LDH and 2.7 eV for NiTi-LDH), which extends the absorption band of LDH to the visible region. We herein established a correlation between the morphology, structure, and composition of an LDH with the photocatalytic activity by utilizing a series of experimental techniques. Therefore, we believe that this study sets an example to reveal the effect of metal-doping on photocatalytic activity.

Author contributions

S. S., S. S. A., and F. K. conceived the project and designed the experiments. S. S. carried out the synthesis, material characterization, and electrochemical measurements. S. S. and S. S. A. performed photocatalytic experiments. S. S. A. and S. S. performed XPS experiments and analysed the data. S. S., S. S. A., and F. K. analysed the data and wrote the manuscript. All authors discussed the results and commented on the manuscript.

Conflicts of interest

There are no conflicts to declare.

Acknowledgements

This work is supported by the Scientific and Technological Research Council of Turkey (TUBITAK), grant number 119C219.

References

1 S. Choudhury, J. O. Baeg, N. J. Park and R. K. Yadav, *Green Chem.*, 2014, **16**, 4389–4400.
2 T. Zhang and W. Lin, *Chem. Soc. Rev.*, 2014, **43**, 5982–5993.
3 R. Nakamura, A. Okamoto, H. Osawa, H. Irie and K. Hashimoto, *J. Am. Chem. Soc.*, 2007, **129**, 9596–9597.
4 X. Lang, X. Chen and J. Zhao, *Chem. Soc. Rev.*, 2013, **43**, 473–486.
5 L. Jing, W. Zhou, G. Tian and H. Fu, *Chem. Soc. Rev.*, 2013, **42**, 9509–9549.
6 Y. Ham, T. Hisatomi, Y. Goto, Y. Moriya, Y. Sakata, A. Yamakata, J. Kubota and K. Domen, *J. Mater. Chem. A*, 2016, **4**, 3027–3033.
7 J. Liu, Y. Liu, N. Liu, Y. Han, X. Zhang, H. Huang, Y. Lifshitz, S. T. Lee, J. Zhong and Z. Kang, *Science*, 2015, **347**, 970–974.
8 N. Fajrina and M. Tahir, *Int. J. Hydrogen Energy*, 2019, **44**, 540–577.
9 Y. W. Chen, J. D. Prange, S. Dühnen, Y. Park, M. Gunji, C. E. D. Chidsey and P. C. McIntyre, *Nat. Mater.*, 2011, **10**, 539–544.
10 X. Ning, W. Zhen, Y. Wu and G. Lu, *Appl. Catal., B*, 2018, **226**, 373–383.
11 Y. Chen, Y. Wang, W. Li, Q. Yang, Q. Hou, L. Wei, L. Liu, F. Huang and M. Ju, *Appl. Catal., B*, 2017, **210**, 352–367.
12 K. H. Ng, S. Y. Lai, C. K. Cheng, Y. W. Cheng and C. C. Chong, *Chem. Eng. J.*, 2021, **417**, 128847.
13 B. Sainbileg, Y. R. Lai, L. C. Chen and M. Hayashi, *Phys. Chem. Chem. Phys.*, 2019, **21**, 26292–26300.
14 C. Noda, Y. Asakura, K. Shiraki, A. Yamakata and S. Yin, *Chem. Eng. J.*, 2020, **390**, 124616.
15 Z. Wu, Y. Liang, X. Yuan, D. Zou, J. Fang, L. Jiang, J. Zhang, H. Yang and Z. Xiao, *Chem. Eng. J.*, 2020, **394**, 124921.
16 L. Liu and A. Corma, *Nat. Rev. Chem.*, 2021, **5**, 256–276.
17 S. Lin, H. Huang, T. Ma and Y. Zhang, *Adv. Sci.*, 2021, **8**, 2002458.
18 S. M. Gupta and M. Tripathi, *Chin. Sci. Bull.*, 2011, **56**, 1639–1657.
19 W. K. Jo, Y. G. Kim and S. Tonda, *J. Hazard. Mater.*, 2018, **357**, 19–29.

20 S. Samuei, Z. Rezvani, A. Shomali, E. Ülker and F. Karadaş, *Eur. J. Inorg. Chem.*, 2020, **2021**, 258–266.
21 S. Samuei, J. Fakkar, Z. Rezvani, A. Shomali and B. Habibi, *Anal. Biochem.*, 2017, **521**, 31–39.
22 S. Samuei, Z. Rezvani and A. R. Amani-Ghadim, *Environ. Prog. Sustainable Energy*, 2017, **36**, 372–381.
23 Y. Zhao, B. Li, Q. Wang, W. Gao, C. J. Wang, M. Wei, D. G. Evans, X. Duan and D. O'Hare, *Chem. Sci.*, 2014, **5**, 951–958.
24 R. K. Sahu, B. S. Mohanta and N. N. Das, *J. Phys. Chem. Solids*, 2013, **74**, 1263–1270.
25 W. Lin and H. Frei, *J. Phys. Chem. B*, 2005, **109**, 4929–4935.
26 Y. Zhao, B. Li, Q. Wang, W. Gao, C. J. Wang, M. Wei, D. G. Evans, X. Duan and D. O'Hare, *Chem. Sci.*, 2014, **5**, 951–958.
27 L. G. Devi and R. Kavitha, *Appl. Catal., B*, 2013, **140–141**, 559–587.
28 G. Liu, L. Wang, H. G. Yang, H. M. Cheng and G. Q. Lu, *J. Mater. Chem.*, 2010, **20**, 831–843.
29 C. G. Silva, Y. Bouizi, V. Fornés and H. García, *J. Am. Chem. Soc.*, 2009, **131**, 13833–13839.
30 K. Parida, L. Mohapatra and N. Baliarsingh, *J. Phys. Chem. C*, 2012, **116**, 22417–22424.
31 D. C. Halvalson, K. H. Ewald, Z. A. Munir, J. Mater Sci, B. Xudong Wang, C. J. Summers, Z. Lin Wang, Z. L. Wang, X. D. Wang and C. J. Summers, *Adv. Mater.*, 2004, **16**, 1215–1218.
32 J. Tang, Z. Zou, J. Ye, J. Ye and Z. Zou, *Angew. Chem.*, 2004, **116**, 4563–4566.
33 L. Wang, W. Chen, D. Zhang, Y. Du, R. Amal, S. Qiao, J. Wu and Z. Yin, *Chem. Soc. Rev.*, 2019, **48**, 5310–5349.
34 T. Wu, S. Sun, J. Song, S. Xi, Y. Du, B. Chen, W. A. Sasangka, H. Liao, C. L. Gan, G. G. Scherer, L. Zeng, H. Wang, H. Li, A. Grimaud and Z. J. Xu, *Nat. Catal.*, 2019, **2**, 763–772.
35 H. Li, L. Zhang, S. Wang and J. Yu, *Int. J. Hydrogen Energy*, 2019, **44**, 28556–28565.
36 M. Asnavandi, Y. Yin, Y. Li, C. Sun and C. Zhao, *ACS Energy Lett.*, 2018, **3**, 1515–1520.
37 T. Zhang, M. Y. Wu, D. Y. Yan, J. Mao, H. Liu, W. Bin Hu, X. W. Du, T. Ling and S. Z. Qiao, *Nano Energy*, 2018, **43**, 103–109.
38 S. Jiang, R. Zhang, H. Liu, Y. Rao, Y. Yu, S. Chen, Q. Yue, Y. Zhang and Y. Kang, *J. Am. Chem. Soc.*, 2020, **142**, 6461–6466.
39 Y. Liu, S. He, Y. Chen, Z. Zou and Q. Wang, *J. Power Sources*, 2021, **506**, 230097.
40 M. Asnavandi, Y. Yin, Y. Li, C. Sun and C. Zhao, *ACS Energy Lett.*, 2018, **3**, 1515–1520.
41 S. Tasleem and M. Tahir, *Energy Fuels*, 2021, **35**, 9727–9746.
42 G. Yang, T. Wang, B. Yang, Z. Yan, S. Ding and T. Xiao, *Appl. Surf. Sci.*, 2013, **287**, 135–142.
43 H. Wang, Y. Yan, Y. S. Mohammed, X. Du, K. Li and H. Jin, *J. Magn. Magn. Mater.*, 2009, **321**, 3114–3119.
44 Y. Zhao, P. Chen, B. Zhang, D. S. Su, S. Zhang, L. Tian, J. Lu, Z. Li, X. Cao, B. Wang, M. Wei, D. G. Evans and X. Duan, *Chem. – Eur. J.*, 2012, **18**, 11949–11958.
45 F. Sarwar, M. Tahir and H. Alias, *Mater. Sci. Semicond. Process.*, 2022, **137**, 106187.
46 S. Tasleem and M. Tahir, *Int. J. Hydrogen Energy*, 2021, **46**, 20995–21012.
47 J. Zhang, J. Liu, L. Xi, Y. Yu, N. Chen, S. Sun, W. Wang, K. M. Lange and B. Zhang, *J. Am. Chem. Soc.*, 2018, **140**, 3876–3879.
48 K. Nejati, Z. Rezvani, M. Mansurfar, A. Mirzaee and M. Mahkam, *Z. Anorg. Allg. Chem.*, 2011, **637**, 1573–1579.
49 D. Kang, X. Yu, M. Ge and W. Song, *Microporous Mesoporous Mater.*, 2015, **207**, 170–178.
50 K. Morimoto, K. Tamura, N. Iyi, J. Ye and H. Yamada, *J. Phys. Chem. Solids*, 2011, **72**, 1037–1045.
51 M. Wei, X. Xu, J. He, Q. Yuan, G. Rao, D. G. Evans, M. Pu and L. Yang, *J. Phys. Chem. Solids*, 2006, **67**, 1469–1476.
52 L. Li, R. Ma, Y. Ebina, K. Fukuda, K. Takada and T. Sasaki, *J. Am. Chem. Soc.*, 2007, **129**, 8000–8007.
53 J. J. Lin and T. Y. Juang, *Polymer*, 2004, **45**, 7887–7893.
54 S. Samuei, F. A. Rad and Z. Rezvani, *Appl. Clay Sci.*, 2020, **184**, 105388.
55 S.-C. Kim, M. S. Islam and S.-J. Hwang, *Sol. RRL*, 2018, **2**, 1800092.
56 F. S. S. Chien, Y. T. Wu, G. L. Lai and Y. H. Lai, *Appl. Phys. Lett.*, 2011, **98**, 153513.
57 R. Abazari, A. R. Mahjoub, S. Sanati, Z. Rezvani, Z. Hou and H. Dai, *Inorg. Chem.*, 2019, **58**, 1834–1849.
58 A. J. Naylor, E. Makkos, J. Maibach, N. Guerrini, A. Sobkowiak, E. Björklund, J. G. Lozano, A. S. Menon, R. Younesi, M. R. Roberts, K. Edström, M. S. Islam and P. G. Bruce, *J. Mater. Chem. A*, 2019, **7**, 25355–25368.
59 F. E. Sarac and U. Unal, *Electrochim. Acta*, 2015, **178**, 199–208.
60 H. Hiroki, F. Kitao and F. Keiichiro, *Chem. Lett.*, 1975, **4**, 409–414.
61 T. Ivanova, A. Naumkin, A. Sidorov, I. Eremenko and M. Kiskin, *J. Electron Spectrosc. Relat. Phenom.*, 2007, **156–158**, 200–203.
62 D. Atzei, A. Rossi and C. Sadun, *Spectrochim. Acta, Part A*, 2000, **56**, 1875–1886.
63 J. L. Gunjakar, T. W. Kim, I. Y. Kim, J. M. Lee and S. J. Hwang, *Sci. Rep.*, 2013, **3**, 1–8.
64 A. Ali Khan and M. Tahir, *Ind. Eng. Chem. Res.*, 2021, **60**, 16201–16223.
65 Y. F. Miao, R. T. Guo, J. W. Gu, Y. Z. Liu, G. L. Wu, C. P. Duan, X. D. Zhang and W. G. Pan, *Appl. Surf. Sci.*, 2020, **527**, 146792.
66 A. Ali Khan and M. Tahir, *Energy Fuels*, 2021, **35**, 8922–8943.
67 L. Fagiolari, M. Bini, F. Costantino, G. Gatto, A. J. Kropf, F. Marmottini, M. Nocchetti, E. C. Wegener, F. Zaccaria, M. Delferro, R. Vivani and A. MacChioni, *ACS Appl. Mater. Interfaces*, 2020, **12**, 32736–32745.
68 C. H. Liu and C. T. Wu, *Colloids Surf., A*, 2010, **353**, 149–156.
69 S. Khan, S. Singh, S. Gaikwad, N. Nawani, M. Junnarkar and S. V. Pawar, *Environ. Sci. Pollut. Res.*, 2020, **27**, 27221–27233.
70 K. G. Akpomie, S. Ghosh, M. Gryzenhout and J. Conradie, *Sci. Rep.*, 2021, **11**, 1–17.
71 J. Tao, Q. Cuan, X. Q. Gong and M. Batzill, *J. Phys. Chem. C*, 2012, **116**, 20438–20446.

72 A. Naldoni, M. Allieta, S. Santangelo, M. Marelli, F. Fabbri, S. Cappelli, C. L. Bianchi, R. Psaro and V. Dal Santo, *J. Am. Chem. Soc.*, 2012, **134**, 7600–7603.
73 F. Sastre, M. Oteri, A. Corma and H. García, *Energy Environ. Sci.*, 2013, **6**, 2211–2215.
74 G. Zhang, B. Lin, W. Yang, S. Jiang, Q. Yao, Y. Chen and B. Gao, *RSC Adv.*, 2014, **5**, 5823–5829.
75 K. Parida, M. Satpathy and L. Mohapatra, *J. Mater. Chem.*, 2012, **22**, 7350–7357.
76 S. Nayak, L. Mohapatra and K. Parida, *J. Mater. Chem. A*, 2015, **3**, 18622–18635.
77 K. Qi, S. Y. Liu and M. Qiu, *Chin. J. Catal.*, 2018, **39**, 867–875.
78 F. Zuo, L. Wang, T. Wu, Z. Zhang, D. Borchardt and P. Feng, *J. Am. Chem. Soc.*, 2010, **132**, 11856–11857.
79 M. Kong, Y. Li, X. Chen, T. Tian, P. Fang, F. Zheng and X. Zhao, *J. Am. Chem. Soc.*, 2011, **133**, 16414–16417.
80 P. R. Chowdhury and K. G. Bhattacharyya, *Photochem. Photobiol. Sci.*, 2017, **16**, 835–839.
81 N. Zhang, M. Q. Yang, S. Liu, Y. Sun and Y. J. Xu, *Chem. Rev.*, 2015, **115**, 10307–10377.
82 S. Velu, K. Suzuki, S. Hashimoto, N. Satoh, F. Ohashi and S. Tomura, *J. Mater. Chem.*, 2001, **11**, 2049–2060.
83 M. Dalal, **https://dalalinstitute.com**.
84 S. S. Akbari and F. Karadas, *ChemSusChem*, 2020, **14**, 679–685.
85 Y. Fu, F. Ning, S. Xu, H. An, M. Shao and M. Wei, *J. Mater. Chem. A*, 2016, **4**, 3907–3913.
86 X. Wang, S. Zhou and L. Wu, *J. Mater. Chem. C*, 2014, **2**, 5752–5758.
87 H. Boumeriame, E. S. Da Silva, A. S. Cherevan, T. Chafik, J. L. Faria and D. Eder, *J. Energy Chem.*, 2022, **64**, 406–431.